Feature Analysis of Blood Spatter Patterns with Image Processing

Thepuli Khemaratne[a]*, Lakmini Malasinghe[a]

[a] *Department of Electrical and Electronic Engineering, Sri Lanka Institute of Information Technology, Malabe 10115, Sri Lanka*

*thepulikhemaratne2003@gmail.com

ABSTRACT

Bloodstain Pattern Analysis (BPA) is a vital component in forensic investigations that aids in reconstructing the sequence of events at a crime scene. It is centralized in and revolves around the categorization of the patterns based on their features, as this is the most significant and critical stage of BPA. Therefore, a preliminary measure of BPA is via the thorough evaluation of images photographed of the crime scene to collect evidence as much as possible to arrive at the correct conclusion and to deduce the relevant details accurately. However, currently existing BPA methods are vulnerable to subjectivity, hence which can lead to pre-assumptions, without thoroughly and completely observing the crime scene, and consequently cause the arrival of incorrect conclusions and discrepancies in BP feature classification. Additionally, other flaws such as unintentional crime scene contamination and evidence tampering exist in these current methods as well. Henceforth, it is imperative that a novel method is constructed to eliminate these issues and arrive at the correct conclusions. This study introduces a robust image-processing-based methodology for extracting and quantifying bloodstain pattern features, thereby enhancing objectivity and reducing human error. The proposed technique encompasses critical stages: image acquisition, preprocessing, segmentation, feature extraction, and analysis. Through the use of image enhancement and segmentation algorithms, essential attributes such as impact angles, tail-to-body ratios, shape irregularities, and distribution densities are computed. The results were validated against original findings and show close agreement in feature values such as convergence area and circularity. The approach demonstrates the potential to integrate with existing BPA tools, facilitating automated, accurate, and reproducible forensic analysis.

KEYWORDS: *Image processing, Forensic science, Bloodstain pattern analysis, Feature extraction, Classification algorithm, Impact angle*

INTRODUCTION

Bloodstain Pattern Analysis is an important forensic technique used to reconstruct and determine the events (including the type of impact, force, weapon, modus operandi, source…etc.) of a crime scene by the analysis of the bloodstain patterns and their features, conducted by forensic scientists, forensic analysists, and investigators (James, Kish, & Sutton, 2005). Effective extraction of these features and their analysis can provide valuable insights into the nature of the incident, the underlying mechanisms, and the aforementioned events/ details of the crime (Siu, Pender, Springer, Tulleners, & Ristenpart, 2017), (Swgstain, 2009). Yet, conventional BPA methods, though widely used, often suffer from subjectivity, potential contamination, and interpretational inconsistencies. Therefore, the need for a robust, impartial, and optimized approach rises, as the reliability of BPA relies heavily on the accuracy and objectivity of pattern interpretation, which remains a challenge due to human bias and potential contamination.

To address the necessity of objectivity in BPA, modern-day developments and advances fixate on incorporating quantitative measures to forensic analysis. Particularly, digital image processing techniques have proven to be powerful tools to enhance the analysis of forensic evidence by the extraction of these aforementioned BP features. These approaches have been successfully applied to various branches of criminology and forensic science, including shoeprint analysis, fingerprint recognition, surveillance footage

https://doi.org/10.54389/LGKX8150

enhancement, and DNA matching. Yet, their application in BPA seems to remain underused (Arthur, et al., 2017), (James, Kish, & Sutton, 2005). From this research paper, an image processing methodology (by following IP techniques and an algorithm) is executed whose main focus and aim is to extract crucial BP features in an automated manner, and therefore increasing the accuracy, precision and efficiency of BPA (Arthur, Cockerton, de Bruin, & Taylor, 2015). This methodology encompasses multiple key image processing steps, such as image acquisition, pre-processing, element segmentation, feature extraction, and the evaluation of the results obtained.

Thus, the intended objectives are as follows:

- To devise an image processing methodology to analyze features of a bloodstain pattern with less complexity, less computational power consumption, and minimal resources to produce results with satisfactory accuracy.
- To deduce the area of convergence to determine the vicinity of origin.

In the first step: image acquisition, unless a pre-existing image is obtained from another source, the original image of the bloodstained surface is typically captured to obtain a high-resolution photograph, by using suitable imaging equipment, i.e., digital cameras. After this image acquisition step, in the preprocessing stage where the image is subjected to quality enhancement and reduction of noise via image filtering, contrast enhancement…etc. (Arthur, et al., 2017).

The ultimate goal of this research is to enhance the objectivity of BPA by the provision of reliable numerical data that can back up their conclusions for credibility. By the devising of a foundation of quantizable features, this methodology is able to contribute to the development of automated classification of BP features. Furthermore, this explores the potential of the fusion of this method with currently existing BPA methods for the improvement of accuracy, precision, and consistency. Thus, the rising demand of the entities involved in forensic science is also addressed, as the subjectivity and partiality are decreased by this method. The aim in this research is to develop the field in forensic science by the exhibition of the value of such methods in BPA, which will henceforth contribute to more reliable and accurate crime reconstructions and evidence analysis (Arthur, et al., 2017).

METHODOLOGY

In this research report, as the data input, the image of the bloodstain pattern which was given in the original research paper itself was used, since due to resource limitations, that was the only option available. Also, to conduct the image processing methodology, only the *MATLAB R2021a* software was used to compile the C++ program. The methodology is depicted in the overview diagram illustrated below in Figure 1:

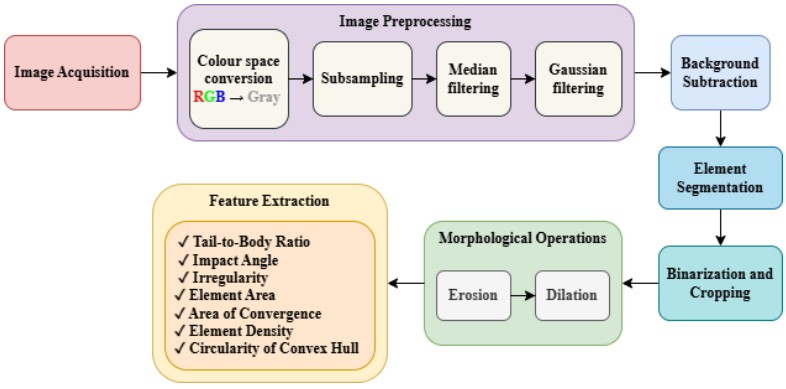

Figure 41. Overview diagram of the Methodology

Image Acquisition

First and foremost, the original image (Figure 2) given in the original/ reference research paper itself was directly extracted due to limitations in resources instead of typically capturing from a new or reenacted/ recreated bloodstained scene using an image capturing device. Secondly, its resolution was measured and compared to that of the original image (Arthur, et al., 2017). Then, it was found that the resolution of this

image was significantly lower than that of the original image, as mentioned in it. Thus, to resize it to its original dimensions and restore it to attempt to increase its resolution, this image was resized to its original dimensions by using the *imresize* function, with the width and height of the original image defined as an array of pixels. (Lazzaro, Murra, & Schwortz, 2013)

Image Preprocessing and Background Subtraction

Secondly, the image pre-processing steps were followed, in order to enhance image quality and suppress noise, ensuring robust feature extraction. First, the extracted image in RGB colour scale was transformed to gray scale, since it eases computational process in image processing, as it is simpler to deal with a single colour plane ranging from 0 – 255 than that of three separate colour planes, and hence increasing the efficiency in the consequent preprocessing steps, reducing the computational load and memory requirements, and easing the visualization (Gonzalez & Woods, 2009).

Figure 42. Extracted image of the bloodstain pattern

Next, it was subjected to subsampling by a factor of 8, where the pixels are removed from the columns and rows eight-folds, and a median filter of a window size of 50 was applied. Then, the subsampled image underwent background estimation via a Gaussian filter with a sigma value of 50. Afterwards, this was subjected to background subtraction from the gray scaled image. The gray scaled image and the background subtracted image are as given under the Results section as Figure 5 and Figure 6 respectively (Arthur, et al., 2017).

Element Segmentation

Thirdly, the brightness/ intensity histogram of the gray scaled image was obtained to perform segmentation of bloodstain elements. Here, the Triangle Thresholding algorithm was used instead of Otsu's Thresholding algorithm, since unlike other thresholding algorithms and typically used Otsu's Thresholding, the Triangle Thresholding also considers weak and subtle foreground intensities, i.e., in this case degraded or faint bloodstains, and performs segmentation on them better as well. This intensity histogram along with the comparison of Triangle and Otsu's Thresholds was acquired as evident in Figure 7 (Arthur, et al., 2017). Additionally, the threshold value for the Triangle Thresholding algorithm was deduced as well.

Subsequently, the gray scaled image was binarized such that the elements are in black colour (0 intensity) and background in white (255 intensity) and cropped along all four borders by a margin of 1 pixel each. Next, the ruler present in the original image was removed by using a white rectangle of appropriate estimated size, resulting in the image given in Figure 8 in the Results section (Arthur, et al., 2017), (Arthur, Cockerton, de Bruin, & Taylor, 2015).

Morphological Operations

Each bloodstain element is typically comprised of a body (the elliptical or circular shaped part) and a tail (thin, elongated end part), as depicted in Figure 3 below:

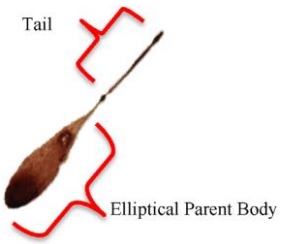

Figure 43. Parts of a typical blood spatter element (a singular bloodstain)

Consequently, the tail parts of each blood spatter element in the pattern was removed by means of morphological operations (Zou & Stern, 2022).
First, the (resultant) cropped binary image was subjected to four iterations of binary erosion using a structuring element of a diamond with the size of 1 pixel defined as $strel$. This eroded image then underwent binary dilation for four iterations as well, using the same aforementioned structing element. This resulted in the removal of the tails of these elements, as evident in Figure 9, which was also restored to its original sizes to preserve its original features as well (Gonzalez & Woods, 2009), (Arthur, et al., 2017).

Feature Extraction

Consequently, the feature extraction steps were followed. Firstly, the tail-to-body ratio of each element was obtained by using equation (1) below. Here, the tail lengths were extracted from the binary cropped image (Figure 8), and the sum of the body length and tail length, i.e., the length of the entire bloodstain element was each obtained from the binary eroded/ dilated image (Figure 9). Consequently, the average tail-to-body ratio of the elements were calculated (Zou & Stern, 2022), (Arthur, et al., 2017).

$$Tail - to - body\ ratio = \frac{Tail\ length}{Body\ length + Tail\ length} \quad (1)$$

Afterwards, the average impact angle (α_{avg}) was calculated from equation (2), by using the width to length ratio. The impact angle is defined as the angle at which a blood droplet has collided/ impacted on a particular surface. It is calculated by incorporating the two axes present/ considered in a bloodstain element: the major axis and the minor axis. The major axis of a bloodstain (element) is defined as the axis across the entire bloodstain, i.e., the axis adjoining the tip of the body and the end of the tail of the bloodstain. Meanwhile, the minor axis can be defined as the width, i.e., maximum distance perpendicular to the major axis adjoining two points of the body of the bloodstain.
The major and minor axes of a typical bloodstain element can be visually depicted according to Figure 3 below:

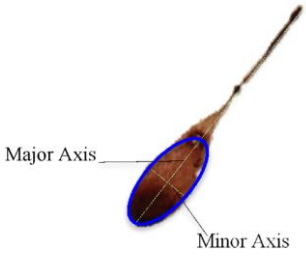

Figure 44. Major and minor axes of a bloodstain element

$$\alpha = \sin^{-1}\left(\frac{Minor\ axis\ length}{Major\ axis\ length}\right) \quad (2)$$

Then, the shapes of the elements were assessed by their irregularity. The irregularity was defined in two ways: by the ratio of the areas of the element and convex hull (Equation (3)), and by the perimeters of the inscribed circle and element body (Equation (4)).

$$Irregularity = \frac{Area\ of\ element}{Area\ of\ convex\ hull} \quad (3)$$

$$Irregularity = \frac{Perimeter\ of\ inscribed\ circle}{Perimeter\ of\ element\ body} \quad (4)$$

The convex hull is defined as the smallest convex region (enclosure comprised of small straight-line segments) that encloses a set of points or a region, which can also be defined as a "rubber band analogy". Alternatively, the convex hull ratio can be described as a degree of how closely the element shape fits/ aligns with its corresponding smooth, convex boundary (Arthur, Cockerton, de Bruin, & Taylor, 2015).
Here, it impartially determines deviations from ideally elliptical/ circular bloodstains which could indicate various types of impacts in several directions or non-linear/ turbulent motion (Arthur, et al., 2017). This ratio ranges from 0 to 1, where ratios closer to 1 indicates smoother/ regular stains that resembles elliptical and circular shapes much more closely. On the contrary, ratios closer to 0 denotes a more irregular/ deviated shape from conventionally elliptical stains.
The inscribed circle can be defined as the circle with the maximum diameter that can be fitted inside the boundary of an element. Similarly, this perimeter ratio also ranges from 0 to 1, where ratios closer to 1 reflects that the element closely resembles circularity/ regularity, whereas ratios closer to 0 signifies that the element shape is irregular, potentially consisting of extrusions/ deformities (Gonzalez & Woods, 2009). Therefore, for each bloodstain element of the pattern, these two ratios were calculated separately. Additionally, the area of each element was calculated by using the foreground pixels of the binary image as well.
To find the area of convergence (Figure 10), thin straight lines of a reasonable length were drawn along the major axes across each bloodstain element to find/ estimate the area of convergence via the congestion of the intersections of these lines, which is defined as the location/ vicinity of the source of blood spatter (James, Kish, & Sutton, 2005), (de bruin, Stoel, & Limborgh, 2011).

Finally, the distribution of the elements within the pattern was assessed. The element distribution is defined in two ways: the circularity of convex hull and the element density. To obtain the circularity value of the convex hull, the binary eroded/ dilated image was used as the input for the function $bwconvhull$, and the area (A) and perimeter (P) of the convex hull were extracted by $regionprops$ function. The circularity is expressed by the Equation (5):

$$Circularity\ of\ the\ convex\ hull = \frac{4\pi A}{P} \quad (5)$$

The element density of the BP was obtained in terms of elements per square cm (Figure 12), and to deduce both the highest and overall element density, a 10 cm × 10 cm box was moved across the BP in 1 cm steps (Zhang & Lu, 2004).

RESULTS

The resolution of the extracted image was found to be **357 × 454 pixels**, and in terms of pixels per mm, it was found to be approximately $\mathbf{3.78\ px./mm}$ **(pixels per mm)**, which was then restored to its original dimensions: **3860 × 4912 pixels (**$\mathbf{10.1\ px/mm}$**)**.
The gray scaled image and the background subtracted image are as follows:

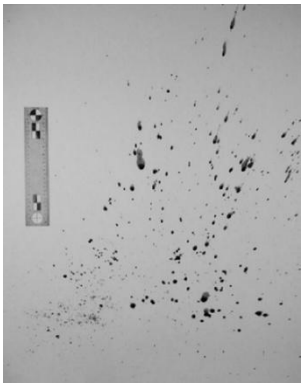

Figure 45. Gray scaled image

Figure 46. Resultant background subtracted image

The obtained intensity histogram of the gray scaled image along with the Otsu's and Triangle Thresholds is displayed beneath:
Additionally, the threshold value for the Triangle Thresholding algorithm was discovered to be **149.**

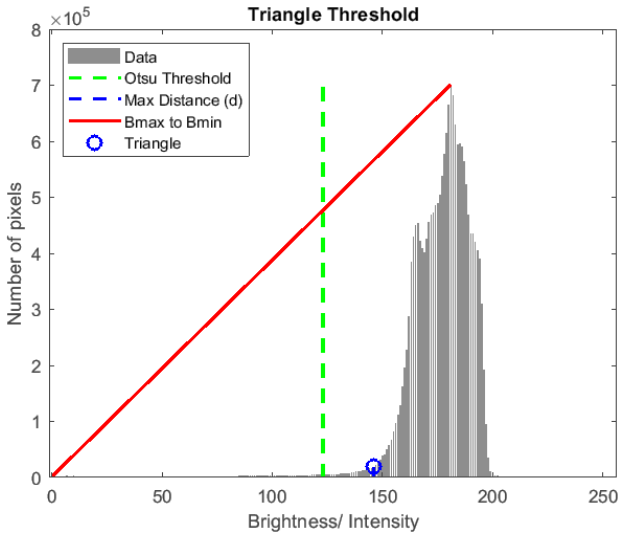

Figure 47. Intensity/ brightness histogram of the gray-scaled image with the Otsu threshold and Triangle threshold indicated

Post binarization and cropping, the image after the elimination of the ruler present is given below:

Figure 48. Binarized and cropped image

The image after the above binarized and cropped image was subjected to the aforementioned morphological operations and restored to its original size is as follows:

Figure 49. Binary eroded/ dilated image

Under the feature extraction steps, the results obtained are as follows:

The tail-to-body ratio of the BP was found to be **0.75**, which indicates that 75% of the body of a bloodstain element is comprised of its tail. The mean impact angle α_{avg} was found to be **46.53°**, which is well within the range of **49.6 ± 17.3°** which was the α_{avg} value obtained in the original source (Arthur, et al., 2017), and can be considered to be approximate to 49.6° as well.

Furthermore, the irregularity in terms of element to convex hull ratio was deduced to be **0.16**, which means that most elements have themselves closely bounded by their convex hulls with lesser blank spaces within those enclosures. Additionally, it was deduced that the mean element area was **0.99 mm^2**.

When straight line segments of significant length were plotted across each bloodstain along their major axes, the following result was obtained. However, it was unable to generate a heat map. Yet, as a rough estimation, the region enclosed below by a box can be considered as this convergence area, and this is quite similar to the area of convergence given per the original source.

Ultimately, the obtained value of the circularity of the convex hull is **0.81**, whereas the original value of the reference was **0.79**, and thus it can be considered that this obtained value is approximate enough to its original value. Also, the highest and overall element densities were **0.96 elements/cm^2** and **0.28 elements/cm^2** respectively, and their respective original values were **1.3 elements/cm^2** and **0.34 elements/cm^2**. Furthermore, it was discovered that the region with the highest element density was at the bottom-left part of the BP.

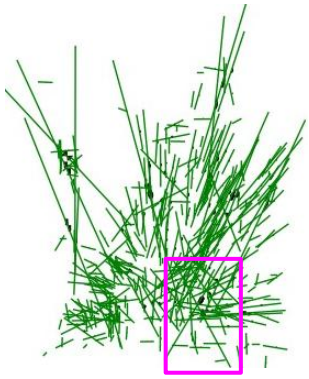

Figure 50. Straight lines drawn across the major axes of the bloodstain elements to deduce the area of convergence

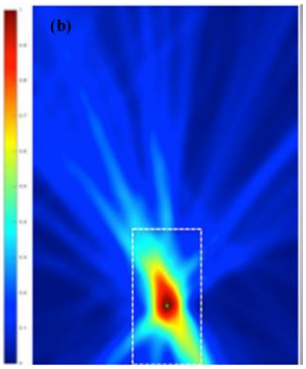

Figure 51. Original heat map with the 'hot spot' for side-by-side comparison and verification of the area of convergence

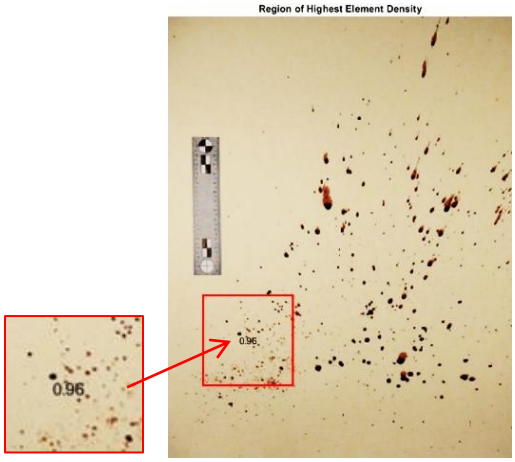

Figure 52. BP with a box enclosing the area with the highest element density

DISCUSSION

The results obtained and depicted above reflect the effectiveness of the adapted image-processing methodology in extracting and analyzing quantitative features of bloodstain patterns. Despite working with an image extracted from a publication (as opposed to a raw high-resolution capture), the feature values achieved closely mirror those in the original study.

In terms of validity and reliability, the close agreement of impact angle, density, and circularity measurements between this study and the original source supports the reliability of the implemented methodology. Minor deviations such as the slightly higher circularity and slightly lower density are likely attributable to image resolution limitations and manual segmentation artifacts. Furthermore, during segmentation, the selection of the Triangle Thresholding algorithm proved effective in isolating faint stains and background elements that would likely have been missed with Otsu's Thresholding algorithm. Additionally, morphological operations preserved the integrity of stain shapes, which was crucial for shape-based feature extraction.

Additionally, in terms of regional context, this methodology was designed in a generalized manner, and hence, it can be implemented anywhere, locally or globally. Also, it has utilized less software tools, where the image resolution was deduced and refinement was conducted in the algorithm itself, and hence, it consumes less computational power and effort, more efficient. Therefore, this can be implemented in rural areas where facilities are scarce as well.

As stated, numerous limitations arose in conducting this methodology, where the preliminary limitation was the inability to generate a heatmap to visualize the convergence area with a highly contrast visual aid.

This was due to the absence of spatial intensity mapping in the implementation. Additionally, because the image was taken from an existing publication (Figure 11) and not acquired through calibrated imaging hardware, there may be scaling inaccuracies despite resizing. Future implementations could overcome this limitation by integrating alternative scaling techniques and adding support for color segmentation and adaptive binarization, improving performance across more diverse datasets.

Other future work for improvement which potentially could affect the process positively include the integration of Machine Learning and Deep Learning (ML/ DL) and Artificial Intelligence (AI) to incorporate multiple inputs for the dataset to train a highly efficient model, which can consequently developed into a non-invasive, automated device/ model that can predict/ determine the modus operandi, crime weapon, or type of impact, as well as a 3D crime scene reconstruction by incorporating stereo imaging for volumetric bloodstain trajectory modeling.

CONCLUSION

In conclusion, throughout this research paper, a unique image-processing procedure is reported on behalf of the assessment of bloodstain patterns and their images acquired. Through this, it was able to obtain quantizable data of the features of both the bloodstain elements and the entire pattern overall as well. The methodology detailed in this is comprehensive and systematic, as the process to extract BP features has been automated. The key stages of this methodology included image acquisition, preprocessing and post-processing, element segmentation, feature extraction, and their analysis and interpretation. Also, the aim of this research, which was to enhance the accuracy, precision, and objectivity and impartiality of the BPA was achieved as well. By incorporating advanced image processing algorithms and techniques, the proposed methodology will greatly contribute to aiding forensic scientists and crime-scene analysts and investigators in crime-scene reconstruction, identifying the MO and weapons, type of impact or trauma, and ultimately to arrive at the correct conclusions.

Furthermore, some of these results were obtained and verified using *Google Colaboratory* for better accuracy as well (Ali, Khan, & Waleed, 2020).

Also, the potential reasons for the minute deviations of the obtained results and that of the original research paper are image quality issues, though the image resolution has been restored to its original resolution/ dimensions. This is possibly due to the image acquisition method, since to conduct this research paper, the image was directly obtained from the original paper instead of creating an arbitrary blood spatter pattern and capturing it with an imaging device such as a digital camera.

REFERENCES

1. Ali, I., Khan, A., & Waleed, M. (2020). A Google Colab Based Online Platform for Rapid Estimation of Real Blur in Single-Image Blind Deblurring. *2020 12th International Conference on Electronics, Computers and Artificial Intelligence (ECAI).* IEEE. https://doi.org/10.1109/ECAI50035.2020.9223244
2. Arthur, R. M., Cockerton, S. L., de Bruin, K. G., & Taylor, M. C. (2015). A novel, element-based approach for the objective classification of bloodstain patterns. (C. Cattaneo, & C. Jackowski, Eds.) *Forensic Science International, 257*, 220 - 228. https://doi.org/10.1016/j.forsciint.2015.08.028
3. Arthur, R. M., Humburg, P. J., Hoogenboom, J., Baiker, M., Taylor, M. C., & Bruin, K. G. (2017). An image-processing methodology for extracting bloodstain pattern features. *Forensic Science International, 277*, 122 - 132. http://dx.doi.org/10.1016/j.forsciint.2017.05.022
4. de bruin, K. G., Stoel, R. D., & Limborgh, J. C. (2011, July 25). Improving the Point of Origin Determination in Bloodstain Pattern Analysis. (M. Peat, Ed.) *Journal of Forensic Sciences, 56*(6), 1476 - 1482. https://doi.org/10.1111/j.1556-4029.2011.01841.x
5. Gonzalez, R. C., & Woods, R. E. (2009). *Digital Image Processing* (Third ed.). Prentice Hall, Pearson Education. https://dl.acm.org/doi/10.5555/1076432
6. James, S. H., Kish, P. E., & Sutton, T. P. (2005). *Principles of Bloodstain Pattern Analysis - Theory and Practice.* Taylor & Francis. https://doi.org/10.1201/9781420039467

7. Lazzaro, P. D., Murra, D., & Schwortz, B. (2013). Pattern recognition after image processing of low-contrast images, the case of the Shroud of Turin. In Z. Duric, & P. Radeva (Ed.), *Pattern Recognition. 46*, pp. 1964 - 1970. Elsevier. https://doi.org/10.1016/j.patcog.2012.12.010
8. Siu, S., Pender, J., Springer, F., Tulleners, F., & Ristenpart, W. (2017). Quantitative Differentiation of Bloodstain Patterns Resulting from Gunshot and Blunt Force Impacts. *Journal of Forensic Sciences, 62*(5), 1166 - 1179. https://doi.org/10.1111/1556-4029.13418
9. Swgstain, S. (2009). Scientific Working Group on bloodstain pattern analysis: recommended terminology. *Forensic Sci Commun, 11*(2), 14 - 17.
10. Zhang, D., & Lu, G. (2004). Review of shape representation and description techniques. *Pattern Recognition. 37'*, pp. 1 - 19. Elsevier. https://doi.org/10.1016/j.patcog.2003.07.008
11. Zou, T., & Stern, H. S. (2022). Towards a likelihood ratio approach for bloodstain pattern analysis. (C. Cattaneo, & C. Jackowski, Eds.) *Forensic Science International, 341*. https://doi.org/10.1016/j.forsciint.2022.111512